FEBS Letters 585 (2011) 3969–3977

FEBS Letters

journal homepage: www.FEBSLetters.org

Following G-quadruplex formation by its intrinsic fluorescence

Nguyen Thuan Dao [a], Reinhard Haselsberger [a,b], Maria-Elisabeth Michel-Beyerle [a,b,*], Anh Tuân Phan [a,*]

[a] Division of Physics and Applied Physics, School of Physical and Mathematical Sciences, Nanyang Technological University, Singapore
[b] Physikalische Chemie, Department Chemie, Technische Universität München, Germany

ARTICLE INFO

Article history:
Received 12 July 2011
Revised 23 October 2011
Accepted 1 November 2011
Available online 10 November 2011

Edited by Michael R. Bubb

Keywords:
Anticancer
DNA
G-quadruplex
Human telomere
Fluorescence

ABSTRACT

We characterized and compared the fluorescence properties of various well-defined G-quadruplex structures. The increase of intrinsic fluorescence of G-rich DNA sequences when they form G-quadruplexes can be used to monitor the folding and unfolding of G-quadruplexes as a function of cations and temperature. The temperature-dependent fluorescence spectra of different G-quadruplexes also exhibit characteristic patterns. Thus, the stability and possibly also the structure of G-quadruplexes can be characterized and distinguished by their intrinsic fluorescence spectra.

1. Introduction

Guanine-rich DNA and RNA sequences can form four-stranded helical structures called G-quadruplexes based on stacking of G•G•G•G tetrads [1–3]. G-quadruplexes formed by natural DNA sequences in the telomeres and oncogenic promoters and by RNA sequences in the 5′ untranslated region (5′UTR) of oncogenic transcripts have been established as attractive anticancer targets [2,4]. On the other hand, engineered G-quadruplexes can have potential applications ranging from medicine to supramolecular chemistry and nanotechnology [1].

G-quadruplex structures are highly polymorphic [1–3]. They give rise to specific spectroscopic signatures in IR [5], UV-absorption thermal difference spectra (TDS) [6,7], CD [8], Raman [9], and NMR [10] spectroscopy. The intrinsic fluorescence yield of DNA is very low [11–14] as it corresponds to quantum yields of the order of $\varphi \sim 10^{-4}$, and the detection of DNA usually relies on targeting DNA selectively with fluorescent dyes [15]. This approach has been used also in search of selective quadruplex binders [16–18]. In analogy to molecular beacons as fluorescent probes in DNA conformational analysis [19], G-quadruplex formation has been followed by pyrene excimer emission [20] and fluorescence resonance energy transfer (FRET) in the ensemble [21,22] and at the single-molecule level [23–25]. In both cases the fluorescent reporters were attached at the termini of DNA sequences. Recently, the detection of G-quadruplex formation using an internal guanine derivative as a fluorescent probe has been reported [26–28]. However, all these strategies involving exogenous fluorophores might affect the G-quadruplex structure [29].

In recent reports [13,14], it has been pointed out that DNA G-quadruplexes have higher intrinsic fluorescence quantum yields than their less-structured counterparts. This notion has been further substantiated by large amplitude, long lifetime components of excited states [14]. Here we confirm these fluorescence properties and focus on the structural aspects of various well-defined G-quadruplexes structures. For all the sequences used in this study, we verified the formation and the structure of G-quadruplexes using NMR, UV absorption and CD spectroscopy [6–8,10]. Using similar DNA concentrations as for UV absorption or CD spectroscopy, we show that the formation of G-quadruplexes as a function of cations and temperature can be followed by their fluorescence and fluorescence excitation spectra. These features are shown to discriminate, for example, between G-quadruplex and Z-DNA structures.

2. Materials and methods

2.1. Sample preparation

DNA oligonucleotides (Table S1) were chemically synthesized on an ABI 394 DNA/RNA synthesizer and purified as previously

Abbreviations: HT, human telomere; NMR, nuclear magnetic resonance; CD, circular dichroism; UV, ultraviolet; TDS, thermal difference spectra

* Corresponding authors at: Division of Physics and Applied Physics, School of Physical and Mathematical Sciences, Nanyang Technological University, Singapore.
E-mail addresses: mariaelisabeth@ntu.edu.sg (M.-E. Michel-Beyerle), phantuan@ntu.edu.sg (A.T. Phan).

0014-5793/$36.00
doi:10.1016/j.febslet.2011.11.004

described [30]. Samples were dialyzed successively against solution containing the respective salt and against water. DNA concentration was expressed in strand molarity using nearest-neighbor approximation for the absorption coefficients of the unfolded species [31].

2.2. NMR spectroscopy

NMR experiments were performed on 600 or 700 MHz Bruker spectrometers at 25 °C. Proton spectra in H_2O were recorded using JR-type pulse sequences for water signal suppression [32,33]. The DNA concentration in NMR samples was typically 0.02–0.5 mM and the aqueous solution contained 10% D_2O.

2.3. Steady-state optical spectroscopy

2.3.1. Absorption spectroscopy

UV absorption measurements were performed at 20 °C using a quartz cuvette with an optical pathlength of 1 cm. The DNA concentration was $\sim 5 \times 10^{-5}$ M per base, unless stated otherwise. UV absorbance was measured using a Varian CARY-300 spectrophotometer. Melting experiments performed on the same instrument monitored the absorption at 295 nm (for G-quadruplex forming sequences) as a function of temperature [6]. Samples were covered with approximately 100 μl of paraffin oil to prevent water evaporation. They were equilibrated at 90 °C for 10 min, then cooled to 20 °C and heated to 90 °C twice consecutively at a rate of 0.2 °C per minute. Data were collected every 1.2 °C during both cooling and heating processes.

2.3.2. Fluorescence spectroscopy

Fluorescence and excitation spectra were recorded on a Jobin-Yvon-Spex Fluorolog 3-11 fluorometer using an optical pathlength of 1 cm in a right angle geometry. All spectra are scanned with an integration time of 0.5 s, an excitation and emission slit width of 4 nm, and step size of 1 nm. The instrument-specific photomultiplier tube correction file supplied by the manufacturer was applied to all spectra. Temperature-dependent fluorescence spectra were acquired either on the Fluorolog 3-11 or on PTI Quanta Master 4 using the same experimental conditions. Temperature control was achieved either by an external circulating water bath NESLAB RTE attached to the sample compartment (PTI Quanta Master 4) or by a Peltier device (Fluorolog 3-11). Samples were covered with approximately 100 μl of paraffin oil to prevent water evaporation. The heating and cooling rates were ~2 °C per minute. The DNA concentration was $\sim 5 \times 10^{-5}$ M per base (or ~2–4 μM in strand), unless stated otherwise.

2.3.3. Correction of fluorescence and fluorescence excitation spectra

In case the optical density exceeds 0.07 at both the excitation and the fluorescence wavelength, OD_{exc} and OD_{em}, the excitation and the emission intensities are attenuated by $10^{-0.5\ OD(exc)}$ and $10^{-0.5\ OD(em)}$ respectively. The corrected fluorescence intensity is given approximately [34] by

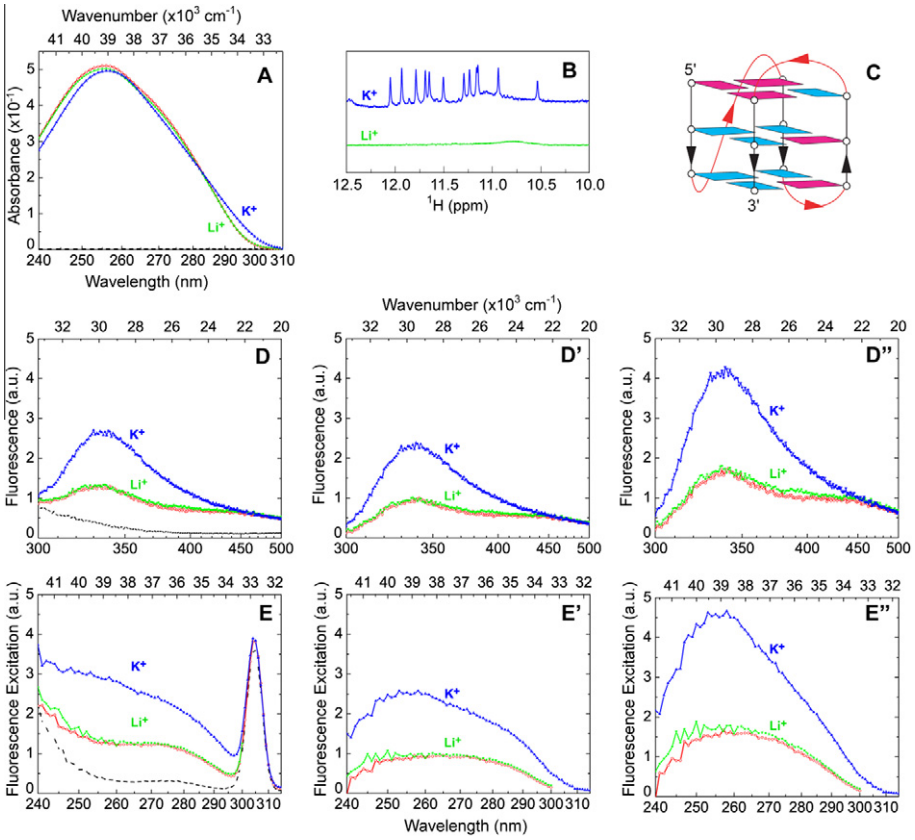

Fig. 1. NMR and optical spectra of the human telomeric d[TT(GGGTTA)$_3$GGGA] sequence (HT). Spectra of HT in different solutions are color-coded as follows: 5 mM Tris–HCl buffer, pH 6.8 (red), after addition of 5 mM LiCl (green), and after further addition of 5 mM KCl (blue). The black dashed curve shows the fluorescence of the bare Tris–HCl buffer. (A) Absorption spectra (in OD). (B) Imino proton NMR spectra (normalized to sugar and aromatic protons). (C) The schematic structure of HT. (D) Fluorescence spectra of HT (λ_{exc} = 260 nm). (D′) Fluorescence spectra D upon subtraction of the Tris-buffer emission. (D″) Fluorescence spectra D′ upon IFE correction. (E, E′, and E″) are the respective fluorescence excitation spectra monitored at 330 nm, with the 295-nm peak in E being the Raman signal of water. Fluorescence and absorption spectra were recorded at 20 °C. The DNA concentration was $\sim 5 \times 10^{-5}$ M per base in fluorescence and UV absorption measurements and $\sim 1 \times 10^{-2}$ M per base in NMR experiments.

$$F_{corr} = F_{obs} \times 10^{(OD_{exc}+OD_{em})/2} \quad (1)$$

accounting for both, the Inner Filter Effect (IFE) and fluorescence reabsorption.

2.3.4. Fluorescence quantum yield measurements

The quantum yield in bare Tris–HCl buffer (pH 6.8) and in the presence of K^+ was measured by using 2′-deoxyguanosine 5′-monophosphate (dGMP) as the reference [34,35]. DNA samples of various concentrations (OD = 0.01–0.1) were used for measurements. The solvent was either deionized water containing 5 mM Tris–HCl buffer only or 5 mM Tris–HCl buffer supplemented with 5 mM KCl. Absorption and fluorescence spectra were recorded using a 1-cm-pathlength cuvette. For fluorescence measurements, samples were excited at 265 nm to match the condition reported in Ref. [35]. The background spectra of the solvent were subtracted from the respective spectra of the samples. The quantum yield was determined using the equation $Q = Q_R\,(\alpha/\alpha_R)$, where Q and Q_R are the quantum yields of the sample and reference, respectively while α and α_R are the slopes of the integrated fluorescence intensity-vs-absorbance for the sample and reference, respectively. For simplicity, we considered the solvent refractive index for the sample (5 mM Tris–HCl buffer) and for the reference (deionized water) to be similar.

2.4. Time-resolved fluorescence measurements

The fluorescence decay at 330 nm was measured using a time-correlated single photon counting (TCSPC) set-up from PicoQuant. The output of a Titan:Sapphire Laser (780 –1000 nm, 80 MHz, 100 fs) was frequency tripled (THG) to obtain a 260-nm excitation and focused onto the sample (peak intensity, 2 $kWcm^{-2}$). A portion of the excitation light was used as the start signal for the measurement cycle controlled by histogram accumulating real-time processor (PicoHarp 300). The spectrometer FluoTime 200 with wavelength resolution of 1 nm or better was used to collect the fluorescence signal. This signal was then recorded by a Multi-Channel-Plate Photomultiplier Tube (MCP-PMT) with an overall IRF (Instrument Response Function) FWHM of 30 ps. The fluorescence decays were fitted using the convolution of the IRF and the multi-exponential decay function with lifetimes τ_i with $i \leqslant 3$:

$$I(t) = \int_{-\infty}^{t} IRF(t') \sum_{i=1}^{n} A_i e^{\frac{t-t'}{\tau_i}} dt' \quad (2)$$

by deconvoluting the recorded signal $I(t)$ (software FluoFit) a time resolution of 15 ps can be achieved.

3. Results and discussion

3.1. Following cation-dependent G-quadruplex formation of human telomeric sequence

Fig. 1(A–E) shows a compilation of structural and spectroscopic data which are representative of unfolded and folded structures of the 24-nt human telomeric sequence d[TT(GGGTTA)$_3$GGGA] (henceforth termed HT). At room temperature, NMR imino protons at 10–12 ppm were observed for HT in K^+ solution, but not in Li^+ solution (Fig. 1B), indicating G-quadruplex formation of this sequence in K^+ solution (Fig. 1C), but not in Li^+ solution. The NMR spectrum observed here in K^+ solution was similar to the one reported previously [36], in which this human telomeric sequence has been determined to form a (3+1) G-quadruplex (Fig. 1C).

Fig. 1A displays the absorption spectra of HT recorded in different solutions: 5 mM Tris–HCl buffer, pH 6.8 (red), after addition of 5 mM LiCl (green), and after further addition of 5 mM KCl (blue). The difference between these absorption spectra (Fig. S1) indicative of G-quadruplex formation in the presence of K^+ is closely related to the absorption thermal difference spectra (TDS) reported in Ref. [7].

Fig. 1D shows the corresponding fluorescence spectra of HT upon excitation at 260 nm. The fluorescence spectra of this sequence in

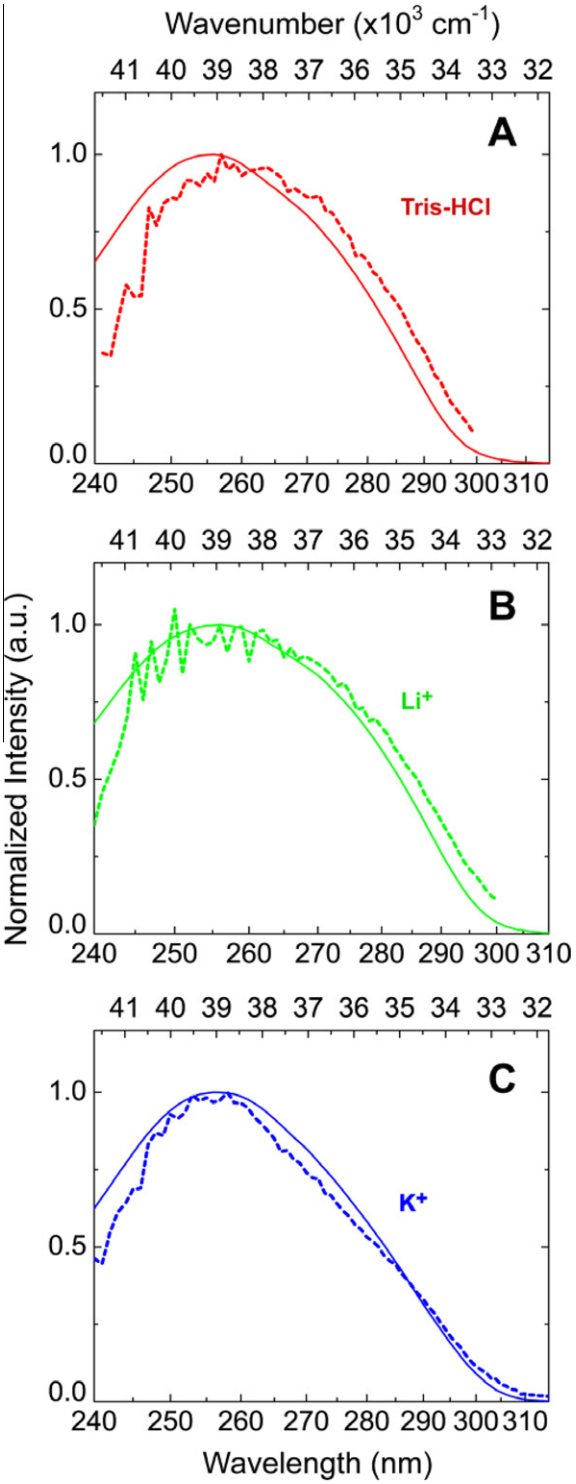

Fig. 2. Comparison between the normalized absorption (continuous line) and the normalized fluorescence excitation (dashed line) spectra of HT in Tris–HCl buffer and in the presence of different cations, Li^+ and K^+: (A) in 5 mM Tris–HCl buffer, pH 6.8; (B) after addition of 5 mM LiCl; (C) after further addition of 5 mM KCl.

Table 1
Quantum yields of G-rich sequences in different buffer solutions.

Sequence	Solvent	Excitation wavelength (nm)	Quantum yield $\times 10^{-4}$	Reference
HT	5 mM Tris–HCl (pH 6.8)	265	1.4 ± 0.1	This work
HT	5 mM Tris–HCl (pH 6.8), 5 mM KCl	265	3.5 ± 0.1	This work
GpG	Phosphate (pH 7)	248	1.3	[45]
polyG	Phosphate (pH 7)	248	4.7	[45]
G_9	10 mM potassium phosphate (pH 7.2), 50 mM KCl	275.5	2.39	[13]
G-wires	30 mM sodium phosphate (pH 7.4), 100 mM NaCl	265	9.5 ± 0.1	[35]

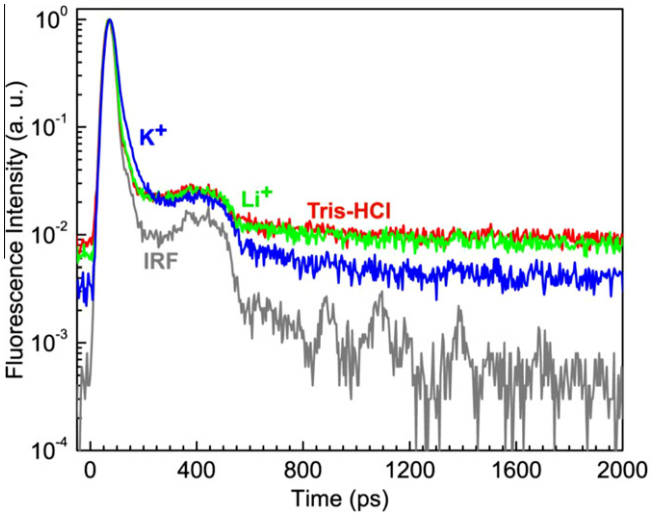

Fig. 3. Fluorescence decay of HT excited at 260 nm and probed at 330 nm in different solutions as encoded in Fig. 1. The instrument response function (IRF) of the (TCSPC) set-up was measured using the Raman emission of water at 285 nm.

bare Tris–HCl buffer and upon adding 5 mM LiCl are strictly superimposed. Further addition of 5 mM KCl leads to the development of a broad unstructured fluorescence band peaking between 330 and 340 nm as reported before [13,14,37]. As a G-quadruplex structure of HT was detected by NMR only in K^+ solution, but not in Li^+ solution [36], we assign this fluorescence band to G-quadruplex formation. It should be noted that the added volumes of LiCl and KCl from high-concentration stocks are small, resulting in a minute change (<0.5%) in sample volume and thus in DNA concentration. The fluorescence spectra of samples obtained by adding K^+ to the Li^+ solution are similar to those containing only K^+ (Fig. S2), consistent with the notion that specific cations (but not simply the ionic strength) are responsible for the G-quadruplex formation. Similar results were also obtained upon excitation in the blue and the red wings of the absorption spectrum (Fig. S3).

Fig. 1E shows an increasing amplitude of an extremely broad and unstructured excitation spectrum, probing the fluorescence at its maximum (340 nm) in K^+ solution. This characteristic increase was only observed upon addition of K^+ ions, but not Li^+ ions. Similar results were obtained, when the fluorescence excitation was probed in the blue and red wings of the fluorescence band (Fig. S4).

Since the fluorescence measurements depicted in the spectra D and E were performed on samples with a large optical density (OD = 0.5), the resulting spectra have to be corrected for emission losses caused by the Inner Filter Effect (IFE). Due to the negligible overlap of absorption and fluorescence spectra, corrections for reabsorption of fluorescence are minimal and were neglected. Fluorescence and excitation spectra were corrected in two consecutive steps: (i) Subtraction of the background emission of the pure Tris–HCl buffer from the measured fluorescence and fluorescence excitation spectra, D and E, yielding now D′ and E′. (ii) Subsequently, the spectra D′ and E′ were corrected for IFE using the approximate Eq. (1). The corrected fluorescence and excitation spectra are shown in Fig. 1 as D″ and E″.

The consequences of correcting the observed spectra D and E are twofold (i) The corrected fluorescence spectra display an increase of amplitude by approximately a factor of two maintaining otherwise the spectral envelope. We note in passing that the IFE corrected fluorescence spectrum D″ still shows a small-amplitude offset-emission in the 450–500 nm range. This unknown emission also reported in the literature, e.g. Ref. [14], responds to a broad excitation band peaking around 325 nm (Fig. S5) that is well beyond the measurable absorption of DNA. At shorter wavelengths, the excitation spectrum follows the absorption contours of DNA. (ii) Apart from a significant increase of amplitude, the IFE-corrected fluorescence excitation spectra follow now the absorption spectra as shown in Fig. 2. The similarity between absorption and fluorescence excitation spectra underlines the notion that the origin of the fluorescence band peaking around 330–340 nm is indeed absorption of DNA rather than of a photodegradation product.

3.2. Fluorescence quantum yield of human telomeric sequence

Using the reported quantum yield reference $(1.3 \pm 0.1) \times 10^{-4}$ of dGMP [35], the plots of the integrated fluorescence intensity vs. absorbance (Fig. S6) allowed us to estimate the quantum yield of HT in bare Tris–HCl buffer and in the presence 5 mM K^+, being $(1.4 \pm 0.1) \times 10^{-4}$ and $(3.5 \pm 0.1) \times 10^{-4}$, respectively. Thus, the quantum yield of HT in bare Tris–HCl buffer was similar to that of dGMP, whereas a 2.7-fold increase in quantum yield was observed when HT formed a G-quadruplex structure in the presence of K^+. The quantum yield obtained here for the HT G-quadruplex is within the limits of the previously reported values ranging from 2.4 to 9.5 $\times 10^{-4}$ (Table 1). The spread of these values may be due to differences in G-quadruplex structures, as well as other experimental conditions.

Table 2
Fitting parameters of the fluorescence decay of HT sequence in Tris–HCl buffer before and after adding different cations.

Buffer	λ_{em}[nm]	A_1	τ_1 [ns]	Fract. int. [%]	Fract.amp.[%]	A_2	τ_2[ns]	Fract.int. [%]	Fract.amp.[%]	A_3	τ_3 [ns]	Fract.int. [%]	Fract.amp.[%]	χ^2
Li^+	330	27	3.5	1.4	<0.1	47	0.45	0.3	<0.1	6594000	⩽0.01	98.3	100.0	1.081
K^+	330	37	1.1	4.3	<0.1	2636	0.05	13.4	1.7	149980	⩽0.01	83.3	98.3	1.119

3.3. Time-resolved fluorescence decay of human telomeric sequence

The excited-state dynamics of the HT sequence in the presence of Li^+ and K^+ ions has been probed using time-correlated single-photon counting (TCSPC), a technique which favors minimal photodegradation of DNA due to the low overall dosis of photons. As most of the HT fluorescence, excited at 260 nm and probed in the 330–340 nm range, decays on the time scale of the IRF of the TCSPC system, the ultrafast time components cannot be resolved and are therefore subsumed within the limiting resolution of 15 ps. Nevertheless, the temporal fluorescence profiles shown in Fig. 3 point to a slightly slower fluorescence decay in the presence of K^+, than in the presence of Li^+. These qualitative results are consistent with previous reports of the excited-state dynamics of single- and double-stranded DNA [12,37–39], G-rich sequence [12,38] as well as G-quadruplexes [14].

The essential difference between the three-exponential fit parameters (Table 2) for the fluorescence decay of HT in Li^+ and K^+ solutions is the observation of a 50 ps component with a small fractional amplitude of ~2% in the case of K^+ as compared to Li^+ which shows only an ultrafast decay. Concomitantly, the fractional amplitudes of the ultrafast components (<15 ps) are 98% in K^+ as compared to 100% in Li^+ solution. We time-resolved also the fluorescence offset in the 450–500 nm region of the steady-state fluorescence spectra D″ in Fig. 1. In contrast to the decay pattern probed at 330 nm, the decay of this background emission in the 450–500 nm is dominated by 2 ns and 500 ps components (Fig. S5). In principle, the origin of this emission might be one or more impurities at low concentration showing up only due to a favorable combination of extinction coefficient and excited state lifetimes. However, since the excitation spectrum of this emission at shorter wavelengths follows the absorption spectrum of HT (Fig. S5), low-lying excited states of DNA might well be involved. For example, already in 1960, n–$\pi*$ transitions have been proposed to exist at the low-energy side of the strong 260-nm π–$\pi*$ absorption band of DNA [40]. Based on electroabsorption spectra the low-energy absorption in the 300-nm region of single-stranded polynucleotides in water/glycerol mixtures has been explained by interaction of n–$\pi*$ and π–$\pi*$ transitions of neighboring bases [41]. Most recently, the weak absorption tail beyond 300 nm observed for DNA single- and double-strands has been attributed to charge-transfer states that are strongly stabilized in aqueous solution [42].

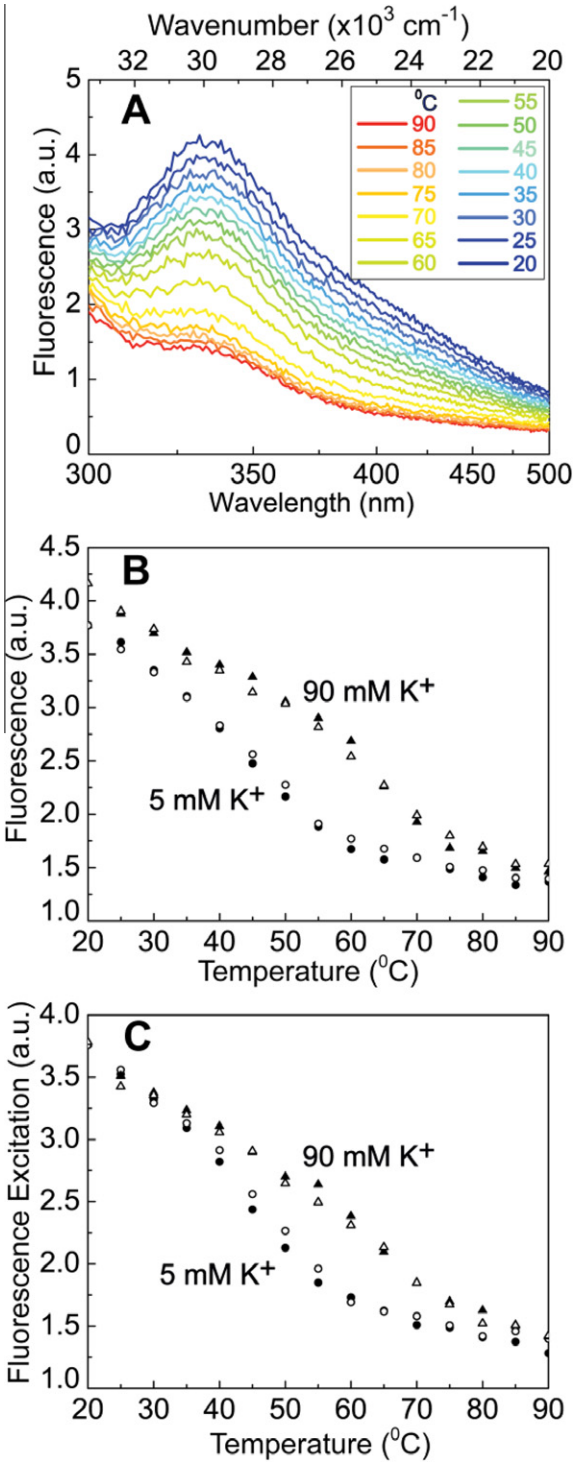

Fig. 4. (A) Temperature dependence of fluorescence spectra of HT in 5 mM Tris–HCl buffer (pH 6.8) supplemented with 5 mM KCl upon excitation at 260 nm. Only the cooling process is shown. (B) 330-nm Peak intensity of fluorescence in the presence of 5 and 90 mM K^+ as a function of temperature. (C) Temperature dependence of the excitation intensity at 260 nm, probed at the 330-nm peak fluorescence of HT in 5 and 90 mM K^+. Full (empty) circles represent the cooling (heating) processes in 5 mM K^+ solution. Full (empty) triangles represent the cooling (heating) processes in 90 mM K^+ solution. The DNA concentration was ~5×10^{-5} M per base.

3.4. Following temperature-dependent G-quadruplex formation of human telomeric sequence

As the formation of G-quadruplexes results in increasing amplitude of the fluorescence, we followed the folding and unfolding of the HT quadruplex by measuring the temperature dependent spectra (Fig. 4A) and plotting the amplitudes of the 330-nm fluorescence vs. temperature as displayed in Fig. 4B. As expected, a similar temperature dependence was observed for the 260-nm fluorescence excitation signals (Fig. 4C). Contributions from temperature-dependent pH-sensitivity of the Tris-buffer can be ignored since similar fluorescence melting results were obtained in Tris–HCl and cacodylate buffer (Fig. S7). These measurements, performed at low (5 mM) and high (90 mM) K^+ concentration, illustrate the role of K^+ concentration on the stability of the G-quadruplex. We emphasize that both, the data of the cooling and heating processes are fully reversible and well-superimposed (Fig. 4). The thermal reversibility of the drastic changes in the fluorescence amplitudes rules out significant contributions from photoproducts accumulating under the experimental conditions of our measurements. The melting characteristics shown in Fig. 4(B and C) are consistent with the ones recorded in UV absorption at 295 nm (Fig. S8), with the melting temperature (T_m) being 50 ± 5 and 60 ± 5 °C for HT at low and high K^+ concentration. In contrast to UV melting curves resting on the loss of the 295-nm hyperchromicity of DNA G-quadruplexes upon unfolding, the melting curves displayed in Fig. 4B and C, are attributed to the decrease of excited state lifetimes upon G-quadruplex unfolding at high

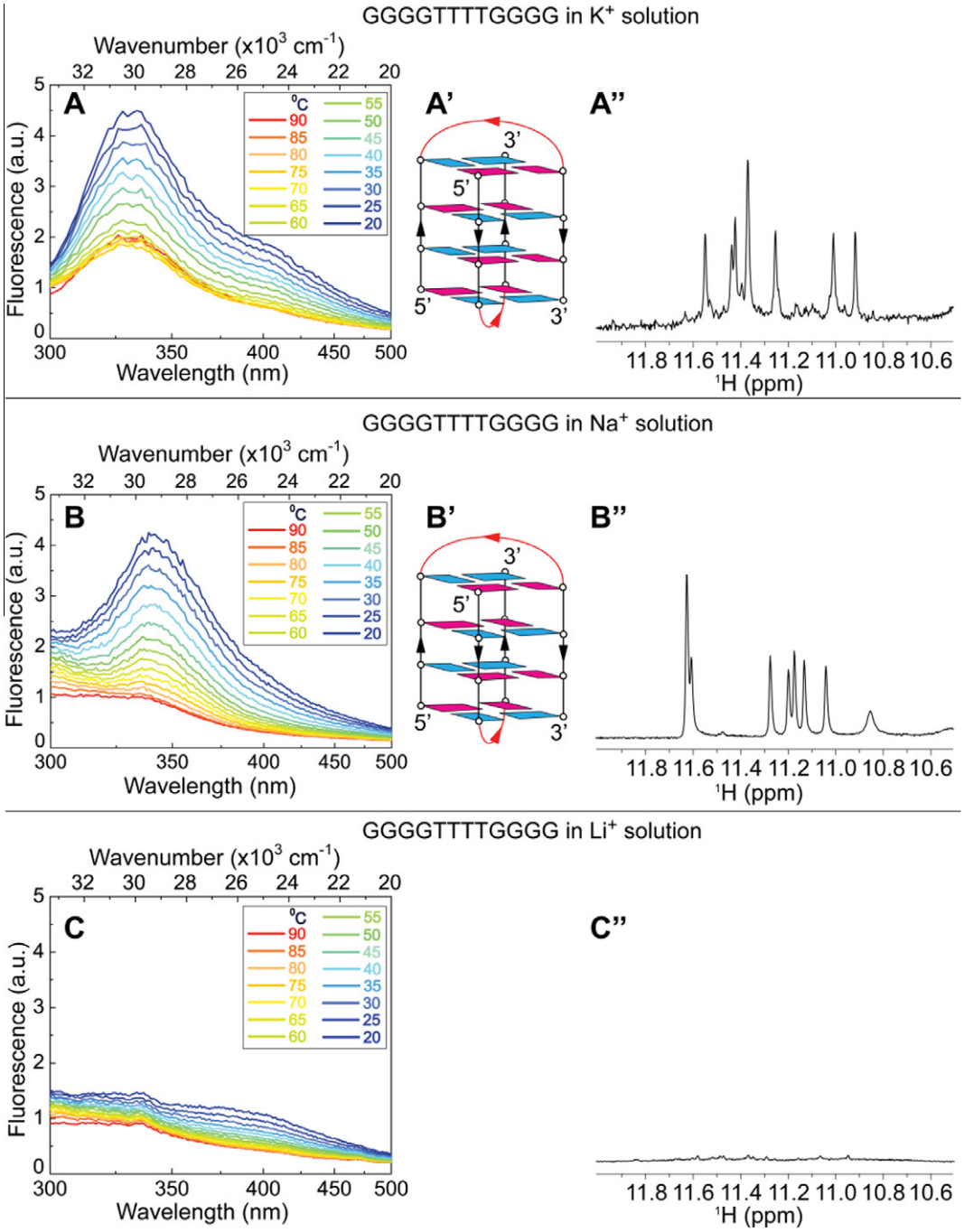

Fig. 5. A-C: Temperature-dependent fluorescence spectra (shown for the cooling process) upon 260-nm excitation of the *Oxytricha* telomeric d(GGGGTTTTGGGG) sequence in different solutions containing 90 mM of (A) K^+, (B) Na^+, and (C) Li^+ at a DNA concentration of $\sim 5 \times 10^{-5}$ M per base. (A′, B′) Schematic structure of G-quadruplexes and (A″–C″) imino proton NMR spectra of *Oxytricha* telomeric d(GGGGTTTTGGGG) sequence in (A″) K^+, (B″) Na^+, and (C″) Li^+ solution. Loops are colored red; *anti* and *syn* guanines are colored cyan and magenta, respectively.

temperature. Detailed studies on temperature-dependent excited state dynamics of DNA structures in different environments are in progress.

3.5. Following G-quadruplex formation of Oxytricha telomeric sequence: effect of cation

In order to find out whether the fluorescence spectra depend on the nature of the cations K^+ and Na^+ in a case where the quadruplex folding is not dependent on the nature of these cations, we recorded temperature-dependent fluorescence spectra of the *Oxytricha* telomeric d(GGGGTTTTGGGG) sequence in K^+, Na^+ and Li^+ solutions (Fig. 5A–C). Here, the formation of the same dimeric basket-type G-quadruplex fold in K^+ and in Na^+ solution (Fig. 5A′, B′) was verified by NMR imino proton spectra (Fig. 5A″, B″), in accordance with the respective NMR spectra reported previously [43]. Fluorescence spectra of d(GGGGTTTTGGGG) in K^+ solution (Fig. 5A) and in Na^+ solution (Fig. 5B) are similar, with the latter being only slightly broader and red-shifted as compared to the former. For the sample in K^+ solution, the 330-nm fluorescence peak was still observed at 90 °C, suggesting the formation of residual higher-order G-quadruplex structures stable at high temperature. Fluorescence spectra of

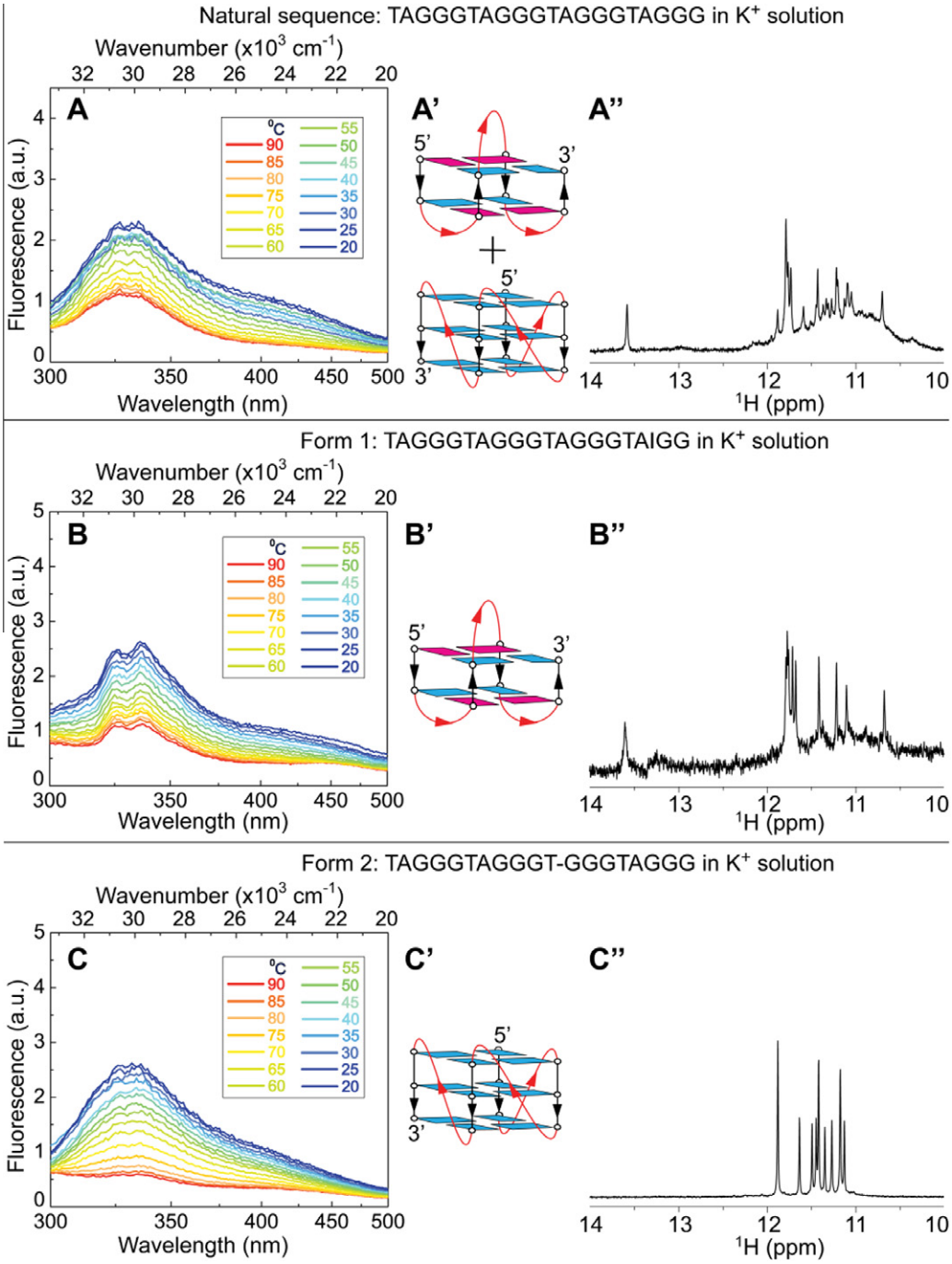

Fig. 6. A-C: Temperature-dependent fluorescence spectra (shown for the cooling process) upon 260-nm excitation of *Giardia* telomeric sequences in three forms: the natural form, d(TAGGG)$_4$, and the modified Forms 1, d(TAGGGTAGGGTAGGGTAIGG), and 2, d(TAGGGTAGGGTGGGTAGGG), all in 90 mM K^+ at a DNA concentration of $\sim 5 \times 10^{-5}$ M per base. (A′-C′) Schematic structures and (A″–C″) imino proton NMR spectra of G-quadruplexes. (A′, A″) natural d(TAGGG)$_4$ sequence; (B′, B″) Form 1, and (C′, C″) Form 2. Loops are colored as in Fig. 5.

d(GGGGTTTTGGGG) in Li^+ solution indicated the lack of G-quadruplex formation (Fig. 5C), consistent with the absence of significant imino proton peaks in the NMR spectrum (Fig. 5C″).

3.6. Following G-quadruplex formation of Giardia telomeric sequence: effect of folding topology

Alternatively, to probe the effect of different G-quadruplex topologies, controlled by the same cation K^+, on the fluorescence spectra, we studied the *Giardia* telomeric d(TAGGG)$_4$ sequence (Fig. 6). This sequence was shown to coexist in two G-quadruplex conformations (Fig. 6A′) in K^+ solution (named Form 1 and Form 2), and each form represents the major structure upon single-residue modification [44]. Substitution of G18 by an inosine favors Form 1, which is a basket-type G-quadruplex containing two G-tetrads, a G•(A-G) triad and two A•T base pairs. Deletion of A12 favors Form 2, which is a propeller-type parallel-stranded G-quadruplex. The formation of these two G-quadruplex conformations was again verified by NMR imino proton spectra (Fig. 6A″-C″). Temperature-dependent fluorescence spectra for the three sequences (natural, Form 1 and Form 2) exhibited a similar extent of fluorescence changes in cooling and heating cycles (Fig. 6A–C). The spectra of

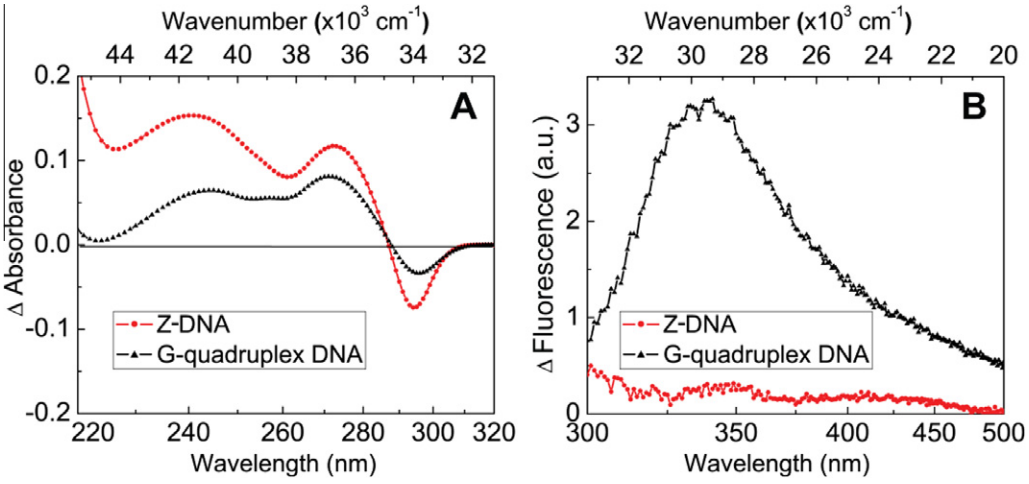

Fig. 7. (A) Absorption and (B) fluorescence thermal difference spectra (TDS) upon 260-nm excitation of Z-DNA (red) and G-quadruplex DNA (black). Z-DNA is formed by the $d(CG)_6$ sequence in 4 M NaCl and G-quadruplex is formed by HT in 5 mM KCl. Absorption TDS [7] were obtained by subtracting the UV absorption spectrum at 20 °C from that at 90 °C while fluorescence TDS were obtained by subtracting the fluorescence spectrum at 90 °C from that at 20 °C. The DNA concentration was $\sim 5 \times 10^{-5}$ M per base in fluorescence and $\sim 8 \times 10^{-5}$ M per base in absorption measurements.

Form 1 and Form 2 showed different fine structures, with two peaks at 325 and 340 nm for Form 1 (Fig. 6B), and only one peak at 330 nm for Form 2 (Fig. 6C). This could reflect the base stacking in the structure of the loops of Form 1. Spectral pattern of the natural sequence resembles to a weighted average between the spectra of Form 1 and Form 2, consistent with this sequence forming a mixture of the two conformations. Residual fluorescence at high temperatures was only observed for the natural and Form 1 sequences, but not for Form 2 sequence.

3.7. Distinction between Z-DNA and G-quadruplex formation

Thus, the intrinsic fluorescence provides a method to identify and follow the G-quadruplex formation complementing other spectroscopic techniques [6–8,10]. For instance, since Z-DNA and G-quadruplex DNA give similar UV-absorption TDS signals [7] at the signature wavelength of 295 nm (Fig. 7A), the two structures can be easily distinguished by their fluorescence thermal difference spectra (Fig. 7B), as the increase in the 330-nm fluorescence signal due to G-quadruplex formation is significantly higher than that due to the formation of a Z-DNA duplex. It should be noted that the DNA strand concentration used in the fluorescence studies here was only ~2 μM, similar to those typically used for UV absorption or CD spectroscopy.

4. Conclusions

Large increase in fluorescence amplitude accompanied by parallel absorption and fluorescence excitation spectra and high reversibility of temperature-dependent fluorescence signals support the notion that these are characteristic features of G-quadruplex structures. Thus, fluorescence spectroscopy constitutes a method for the identification of G-quadruplex formation. Fluorescence spectroscopy is shown to complement other spectroscopic techniques and to provide independent information on specific NMR structures, as well as on the stability and polymorphism of G-quadruplexes.

Sources of funding

Singapore Biomedical Research Council Grant 07/1/22/19/542 and Ministry of Education Grants (ARC30/07 and RG62/07) to A.T.P.

Acknowledgements

We thank Prof. Alfred Huang Cheng Hon for his support and many helpful discussions and Dr. Gagik Gurzadyan, in particular, for useful comments concerning potential photodegradation of DNA. We are indebted to Dr. Tze Chien Sum, Edbert Jarvis Sie and Ricksen Surya Winardi for their participation and help in the early stage of the project.

Appendix A. Supplementary data

Supplementary data associated with this article can be found, in the online version, at doi:10.1016/j.febslet.2011.11.004.

References

[1] Davis, J.T. (2004) G-quartets 40 years later: From 5'-GMP to molecular biology and supramolecular chemistry. Angewandte Chemie-Int. Ed. 43, 668–698.
[2] Patel, D.J., Phan, A.T. and Kuryavyi, V. (2007) Human telomere, oncogenic promoter and 5'-UTR G-quadruplexes: Diverse higher order DNA and RNA targets for cancer therapeutics. Nucleic Acids Res. 35, 7429–7455.
[3] Neidle, S. (2009) The structures of quadruplex nucleic acids and their drug complexes. Curr. Opin. Struct. Biol. 19, 239–250.
[4] Balasubramanian, S. and Neidle, S. (2009) G-quadruplex nucleic acids as therapeutic targets. Curr. Opin. Chem. Biol. 13, 345–353.
[5] Gabelica, V., Rosu, F., De Pauw, E., Lemaire, J., Gillet, J.C., Poully, J.C., Lecomte, F., Gregoire, G., Schermann, J.P. and Desfrancois, C. (2008) Infrared signature of DNA G-quadruplexes in the gas phase. J. Am. Chem. Soc. 130, 1810–1811.
[6] Mergny, J.L., Phan, A.T. and Lacroix, L. (1998) Following G-quartet formation by UV-spectroscopy. FEBS Lett. 435, 74–78.
[7] Mergny, J.L., Li, J., Lacroix, L., Amrane, S. and Chaires, J.B. (2005) Thermal difference spectra: a specific signature for nucleic acid structures. Nucleic Acids Res. 33, e138.
[8] Kypr, J., Kejnovska, I., Renciuk, D. and Vorlickova, M. (2009) Circular dichroism and conformational polymorphism of DNA. Nucleic Acids Res. 37, 1713–1725.
[9] Miura, T. and Thomas, G.J. (1994) Structural polymorphism of telomere DNA - interquadruplex and duplex-quadruplex conversions probed by Raman-spectroscopy. Biochemistry 33, 7848–7856.
[10] Feigon, J., Sklenar, V., Wang, E., Gilbert, D.E., Macaya, R.F. and Schultze, P. (1992) H-1-NMR spectroscopy of DNA. Methods Enzymol. 211, 235–253.
[11] Markovitsi, D., Gustavsson, T. and Sharonov, A. (2004) Cooperative effects in the photophysical properties of self-associated triguanosine diphosphates. Photochem. Photobiol. 79, 526–530.
[12] Gepshtein, R., Huppert, D., Lubitz, I., Amdursky, N. and Kotlyar, A.B. (2008) Radiationless transitions of G4 wires and dGMP. J. Phys. Chem. C 112, 12249–12258.
[13] Mendez, M.A. and Szalai, V.A. (2009) Fluorescence of unmodified oligonucleotides: a tool to probe G-quadruplex DNA structure. Biopolymers 91, 841–850.
[14] Miannay, F.A., Banyasz, A., Gustavsson, T. and Markovitsi, D. (2009) Excited states and energy transfer in G-quadruplexes. J. Phys. Chem. C 113, 11760–11765.

[15] Lakowicz, J.R., Shen, B., Gryczynski, Z., D'Auria, S. and Gryczynski, I. (2001) Intrinsic fluorescence from DNA can be enhanced by metallic particles. Biochem. Biophys. Res. Commun. 286, 875–879.
[16] Monchaud, D. and Teulade-Fichou, M.P. (2008) A hitchhiker's guide to G-quadruplex ligands. Org. Biomol. Chem. 6, 627–636.
[17] Alzeer, J., Vummidi, B.R., Roth, P.J.C. and Luedtke, N.W. (2009) Guanidinium-modified phthalocyanines as high-affinity G-quadruplex fluorescent probes and transcriptional regulators. Angewandte Chemie-Int. Ed. 48, 9362–9365.
[18] Yang, P., De Cian, A., Teulade-Fichou, M.P., Mergny, J.L. and Monchaud, D. (2009) Engineering bisquinolinium/thiazole orange conjugates for fluorescent sensing of G-quadruplex DNA. Angewandte Chemie-Int. Ed. 48, 2188–2191.
[19] Venkatesan, N., Seo, Y.J. and Kim, B.H. (2008) Quencher-free molecular beacons: a new strategy in fluorescence based nucleic acid analysis. Chem. Soc. Rev. 37, 648–663.
[20] Dembska, A. and Juskowiak, B. (2010) Effect of metal cations on the fluorescence lifetimes of pyrene-labeled G-quadruplex probes. J. Photochemi. Photobiol. A-Chem. 212, 36–42.
[21] Mergny, J.L. and Maurizot, J.C. (2001) Fluorescence resonance energy transfer as a probe for G-quartet formation by a telomeric repeat. Chem Bio Chem 2, 124–132.
[22] Green, J.J., Ying, L.M., Klenerman, D. and Balasubramanian, S. (2003) Kinetics of unfolding the human telomeric DNA quadruplex using a PNA trap. J. Am. Chem. Soc. 125, 3763–3767.
[23] Ying, L.M., Green, J.J., Li, H.T., Klenerman, D. and Balasubramanian, S. (2003) Studies on the structure and dynamics of the human telomeric G quadruplex by single-molecule fluorescence resonance energy transfer. Proc. Natl Acad. Sci. USA 100, 14629–14634.
[24] Lee, J.Y., Okumus, B., Kim, D.S. and Ha, T.J. (2005) Extreme conformational diversity in human telomeric DNA. Proc. Natl. Acad. Sci. USA 102, 18938–18943.
[25] Okamoto, K., Sannohe, Y., Mashimo, T., Sugiyama, H. and Terazima, M. (2008) G-quadruplex structures of human telomere DNA examined by single molecule FRET and BrG-substitution. Bioorg. Med. Chem. 16, 6873–6879.
[26] Dumas, A. and Luedtke, N.W. (2010) Cation-mediated energy transfer in G-quadruplexes revealed by an internal fluorescent probe. J. Am. Chem. Soc. 132, 18004–18007.
[27] Dumas, A. and Luedtke, N.W. (2011) Highly fluorescent guanosine mimics for folding and energy transfer studies. Nucleic Acids Res. 39, 6825–6834.
[28] Nadler, A., Strohmeier, J. and Diederichsen, U. (2011) 8-Vinyl-2'-deoxyguanosine as a fluorescent 2 '-deoxyguanosine mimic for investigating DNA hybridization and topology. Angewandte Chemie-Int. Ed. 50, 5392–5396.
[29] Ford, K.G. and Neidle, S. (1995) Perturbations in DNA-structure upon interaction with porphyrins revealed by chemical probes, DNA footprinting and molecular modeling. Bioorg. Med. Chem. 3, 671–677.
[30] Lim, K.W., Alberti, P., Guedin, A., Lacroix, L., Riou, J.F., Royle, N.J., Mergny, J.L. and Phan, A.T. (2009) Sequence variant $(CTAGGG)_n$ in the human telomere favors a G-quadruplex structure containing a G.C.G.C tetrad. Nucleic Acids Res. 37, 6239–6248.
[31] Cantor, C.R., Warshaw, M.M. and Shapiro, H. (1970) Oligonucleotide interactions. 3. Circular dichroism studies of conformation of deoxyoligonucleotides. Biopolymers 9, 1059–1077.
[32] Plateau, P. and Gueron, M. (1982) Exchangeable proton NMR without base-line distortion, using new strong-pulse sequences. J. Am. Chem. Soc. 104, 7310–7311.
[33] Phan, A.-T., Guéron, M. and Leroy, J.-L. (2001) Investigation of unusual DNA motifs. Methods Enzymol. 338, 341–371.
[34] Lakowicz, J.R. (2006) Principles of fluorescence spectroscopy, Springer, New York.
[35] Changenet-Barret, P., Emanuele, E., Gustavson, T., Improta, R., Kotlyar, A.B., Markovitsi, D., Vaya, I., Zakrzewska, K. and Zichich, D. (2010) Optical properties of Guanine nanowires: experimental and theoretical study. J. Phys. Chem. C 114, 14339–14346.
[36] Luu, K.N., Phan, A.T., Kuryavyi, V., Lacroix, L. and Patel, D.J. (2006) Structure of the human telomere in K^+ solution: An intramolecular (3+1) G-quadruplex scaffold. J. Am. Chem. Soc. 128, 9963–9970.
[37] Vayá, I., Gustavsson, T., Miannay, F.A., Douki, T. and Markovitsi, D. (2010) Fluorescence of natural DNA: from the femtosecond to the nanosecond time scales. J. Am. Chem. Soc. 132, 11834–11835.
[38] Schwalb, N.K. and Temps, F. (2008) Base sequence and higher-order structure induce the complex excited-state dynamics in DNA. Science 322, 243–245.
[39] Middleton, C.T., de La Harpe, K., Su, C., Law, Y.K., Crespo-Hernandez, C.E. and Kohler, B. (2009) DNA excited-state dynamics: from single bases to the double helix. Annu. Rev. Phys. Chem. 60, 217–239.
[40] Rich, A. and Kasha, M. (1960) The n- $\pi*$ transition in nucleic acids and polynucleotides. J. Am. Chem. Soc. 82, 6197–6199.
[41] Krawczyk, S. and Luchowski, R. (2007) Electronic excited states of polynucleotides: A study by electroabsorption spectroscopy. J. Phys. Chem. B 111, 1213–1221.
[42] Banyasz, A., Vaya, I., Changenet-Barret, P., Gustavsson, T., Douki, T. and Markovitsi, D. (2011) Base pairing enhances fluorescence and favors cyclobutane dimer formation induced upon absorption of UVA radiation by DNA. J. Am. Chem. Soc. 133, 5163–5165.
[43] Schultze, P., Hud, N.V., Smith, F.W. and Feigon, J. (1999) The effect of sodium, potassium and ammonium ions on the conformation of the dimeric quadruplex formed by the Oxytricha nova telomere repeat oligonucleotide $d(G_4T_4G_4)$. Nucleic Acids Res. 27, 3018–3028.
[44] Hu, L.Y., Lim, K.W., Bouaziz, S. and Phan, A.T. (2009) Giardia telomeric sequence $d(TAGGG)_4$ forms two intramolecular G-quadruplexes in K^+ solution: effect of loop length and sequence on the folding topology. J. Am. Chem. Soc. 131, 16824–16831.
[45] Vigny, P. and Ballini, J.P. (1977) Excited states of nucleic acids at 300 K and electronic energy transfer in: Excited States in Organic Chemistry and Biochemistry (Pullman, B. and Goldblum, N., Eds.), pp. 1–13, Reidel, Dordrecht.